

Analytic Continual Test-Time Adaptation for Multi-Modality Corruption

Yufei Zhang
South China University of Technology
Guangzhou, China
yufeizhang280@gmail.com

Yicheng Xu
Institute of Science Tokyo
Tokyo, Japan
yxu040@e.ntu.edu.sg

Hongxin Wei
Southern University of Science and
Technology
Shenzhen, China
weihx@sustech.edu.cn

Zhiping Lin
Nanyang Technological University
Singapore
EZPLin@ntu.edu.sg

Xiaofeng Zou
South China University of Technology
Guangzhou, China
zouxiaofeng@scut.edu.cn

Cen Chen
South China University of Technology
Guangzhou, China
chencen@scut.edu.cn

Huiping Zhuang
South China University of Technology
Guangzhou, China
hpzhuang@scut.edu.cn

ABSTRACT

Test-Time Adaptation (TTA) enables pre-trained models to bridge the gap between source and target datasets using unlabeled test data, addressing domain shifts caused by corruptions like weather changes, noise, or sensor malfunctions in test time. Multi-Modal Continual Test-Time Adaptation (MM-CTTA), as an extension of standard TTA, further allows models to handle multi-modal inputs and adapt to continuously evolving target domains. However, MM-CTTA faces critical challenges such as catastrophic forgetting and reliability bias, which are rarely addressed effectively under multi-modal corruption scenarios. In this paper, we propose a novel approach, Multi-modality Dynamic Analytic Adapter (MDAA), to tackle MM-CTTA tasks. MDAA introduces analytic learning—a closed-form training technique—through Analytic Classifiers (ACs) to mitigate catastrophic forgetting. Furthermore, we design the Dynamic Late Fusion Mechanism (DLFM) to dynamically select and integrate reliable information from different modalities. Extensive experiments show that MDAA achieves state-of-the-art performance across the proposed tasks.

CCS CONCEPTS

• **Computing methodologies** → **Computer vision tasks; Online learning settings.**

KEYWORDS

Test-Time Adaptation; Multi-Modality; Continual Learning; Analytic Learning

ACM Reference Format:

Yufei Zhang, Yicheng Xu, Hongxin Wei, Zhiping Lin, Xiaofeng Zou, Cen Chen, and Huiping Zhuang. 2025. Analytic Continual Test-Time Adaptation for Multi-Modality Corruption. In *Proceedings of Proceedings of the 33rd ACM International Conference on Multimedia (MM '25)*. ACM, New York, NY, USA, 13 pages. <https://doi.org/10.1145/3746027.3755545>

1 INTRODUCTION

Test-Time Adaptation (TTA) aims to enable pre-trained models to bridge the gap between the source domain and the target domain [15, 23]. Unlike Unsupervised Domain Adaptation (UDA) [29], TTA performs adaptation without any source data (*i.e.*, pre-trained dataset), which not only saves computational resources by avoiding retraining but also preserves the privacy of the source data. One key application of TTA is to address the problem of domain shift from source data to corrupted test data, where the corruption is often caused by weather changes, ambient noise or sensor malfunctions. In these scenarios, Multi-Modal Test-Time Adaptation (MM-TTA) offers a distinct advantage over mono-modal TTA, as domain shifts often affect only a subset of modalities, while others remain relatively stable and informative [20, 27]. This allows the model to leverage uncorrupted modalities to guide adaptation, thereby enhancing robustness in complex real-world environments.

To better reflect real-world settings where distribution shifts are continuous and multi-faceted, Multi-Modal Continual Test-Time Adaptation (MM-CTTA) has been proposed [2]. MM-CTTA addresses more complicated domain shifts, where the target distribution evolves both over time and across modalities. This setting is common in real-world scenarios, particularly for general-purpose AI agents (e.g., autonomous driving, robotic systems) that rely on multiple sensors for perception, as illustrated in Figure 1.A. However, achieving reliable MM-CTTA remains challenging, mainly

Permission to make digital or hard copies of all or part of this work for personal or classroom use is granted without fee provided that copies are not made or distributed for profit or commercial advantage and that copies bear this notice and the full citation on the first page. Copyrights for components of this work owned by others than the author(s) must be honored. Abstracting with credit is permitted. To copy otherwise, or republish, to post on servers or to redistribute to lists, requires prior specific permission and/or a fee. Request permissions from permissions@acm.org.
MM '25, October 27–31, 2025, Dublin, Ireland.

© 2025 Copyright held by the owner/author(s). Publication rights licensed to ACM.
ACM ISBN 979-8-4007-2035-2/2025/10...\$15.00
<https://doi.org/10.1145/3746027.3755545>

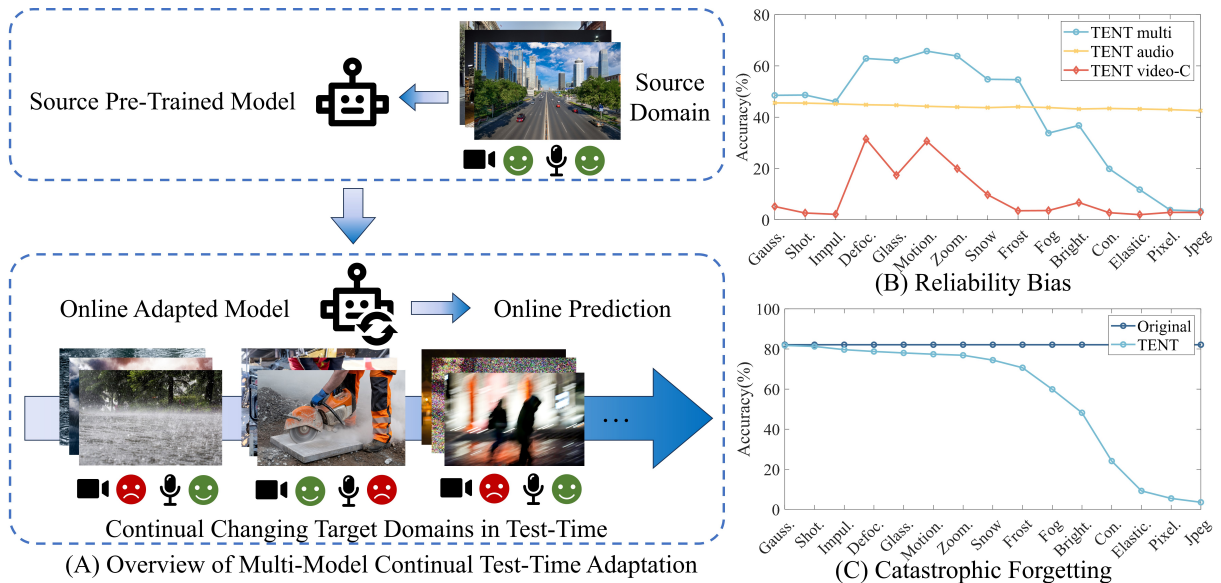


Figure 1: (A) Overview of MM-CTTA. The pre-trained model is initially optimized on source data. During the test-time adaptation phase, however, it must continuously adapt to corrupted data arising from diverse real-world conditions (e.g., weather variations, ambient noise, or sensor malfunctions). **(B-C) Illustration of key challenges in MM-CTTA, using the representative TTA method TENT [23] with CAV-MAE [9] as the backbone.** **(B) Reliability bias:** As the dominant modality (video) becomes increasingly corrupted, the performance of the multi-modal network deteriorates, even falling below that of the audio-only network. **(C) Catastrophic forgetting:** The model’s performance on the source data significantly declines during continuous adaptation. The “Original” refers to the model’s performance on the clean test set of Kinetics50 without any adaptation, while “TENT” represents the performance on the same dataset after adaptation to the corresponding corruption.

due to two key issues. The first is **reliability bias**, which arises from intra-modality domain shifts and exacerbates inconsistencies within downstream fusion networks [27]. The second is **catastrophic forgetting**, where knowledge acquired from the source domain deteriorates during continual adaptation, ultimately reducing the model’s generalization capability [16].

MM-CTTA models must continuously adapt to multi-modal domain shifts while mitigating modality collapse and ensuring reliability in real-world scenarios. While recent researches on TTA have achieving promising results of in **catastrophic forgetting** [7, 18, 24] and **reliability bias** [14, 27] respectively, directly combining CTTA methods with MM-TTA works often falls short. This is because dynamically changing corruption patterns magnify **reliability bias** and create additional complexities, as corruption can unpredictably switch between modalities during continual adaptation. Methods explicitly designed for MM-CTTA remain scarce. The closest existing approach, CoMAC [2], focuses primarily on segmentation tasks in dynamic environments rather than addressing modality corruption.

In this paper, we propose a new approach named **Multi-modality Dynamic Analytic Adaptor (MDAA)** to address the challenges in MM-CTTA. MDAA mainly comprises two primary components: (i) the Analytic Classifiers (ACs), and (ii) the Dynamic Late Fusion Mechanism (DLFM). The ACs update the model by addressing a recursive ridge regression problem, optimizing on both new target data and learned knowledge to avoid **catastrophic forgetting**, such approach have already been used in continual learning (CL)

field [34, 35]. Moreover, each feature type in the multi-modal model is configured with an individual AC in our framework. As a result, MDAA can derive predictions not only from the downstream fusion network but also from the feature encoders, marking a significant departure from conventional multi-modal paradigms.

To effectively utilize outputs from different ACs, we proposed a tailored late fusion strategy, DLFM, which compensates for and integrates predictions across modalities. DLFM selects reliable predictions from modality-specific ACs and propagates them to guide the updates of ACs associated with corrupted modalities, thereby alleviating **reliability bias**. To rigorously assess the robustness and adaptability of MDAA, we design two challenging evaluation settings: (1) adaptation over extremely long phases and (2) scenarios with alternating modality corruption. These settings provide a rigorous test of MDAA’s robustness and adaptability under real-world conditions. The key contributions of this work are listed as follows:

- 1). We introduce ACs to TTA into the TTA framework to prevent the model from **catastrophic forgetting**. We propose DLFM to adaptively fuse features from multiple modalities, thereby mitigating **reliability bias**.

- 2). We design two MM-CTTA benchmarks featuring modality corruption switching and prolonged adaptation, better capturing real-world dynamics, pushing the boundaries of MM-CTTA.

- 3). MDAA achieves state-of-the-art performance, outperforming prior methods by up to 6.22% and 6.84% in two benchmarks, while being more efficient in runtime and memory usage.

2 RELATED WORKS

2.1 Test-Time Adaptation

TTA focuses on enabling a pre-trained model to adapt to a new target domain without requiring access to the source domain data. However, simply relying on incorrect predictions during adaptation can mislead the update process, potentially leading to model collapse [3]. TENT, as one of the first methods solve such issue, addresses this by only updating the model’s batch normalization (BN) layers through entropy minimization [23]. Subsequent research [8, 19, 32] has further mitigated this issue by filtering out low-confidence predictions using carefully designed thresholds and updating the layer normalization (LN) layers for more robust performance.

2.2 Multi-modality Test-Time Adaptation

MM-TTA [11, 25, 27, 31] seeks to enhance model reliability by incorporating multi-modal data into the TTA task. However, imbalances in inter-modal reliability can result in significant performance degradation, known as reliability bias [25], shown in Figure 1.B. Existing MM-TTA models address this issue by independently updating BN or LN layers of each feature encoder, followed by a weighted fusion mechanisms [2, 21, 26]. Although this allows more reliable modalities to carry more weight during fusion, the approach remains relatively shallow in terms of information integration.

A recent model called READ [27] introduced a more advanced approach by fusing features through a Vision Transformer (ViT) [5] block, which allows for the preservation of parameters inherited from source data while effectively integrating inter-modal information [9, 22]. READ achieves reliable adaptation by modulating only the fusion layer within the attention module of the ViT block. Follow-up work [14] aimed to improve performance by updating both the feature encoders and the fusion layer. However, this approach requires prior knowledge about which modalities are corrupted, making it less capable for real-world scenario.

2.3 Analytic Continual Learning

When extending TTA to a continual setting, a significant challenge that emerges is catastrophic forgetting—a phenomenon where adaptation to the target domain leads to degradation of knowledge learned from the source domain and compromises generalization (as illustrated in Figure 1.C). Recent works have explored the integration of Continual Learning (CL) into TTA, demonstrating promising results [2, 18]. Following this line of research, we incorporate a novel CL paradigm, Analytic Continual Learning (ACL), into our proposed MDAA framework.

ACL provides a global optimal solution through matrix inverse operations [10]. To address the out-of-memory issue caused by large inverse matrices, [33] demonstrated that iterative computation using block-wise data achieves results equivalent to joint computation, making analytic learning highly effective in continual learning. By treating data from different time periods as blocks, ACL allows for recursive computation, with the final result being as accurate as if all data were processed simultaneously. Thanks to its non-forgetting properties, ACL has shown strong performance across various CL tasks in recent years [34, 35].

3 MULTI-MODALITY DYNAMIC ANALYTIC ADAPTER

In this section, we first formalize the MM-CTTA problem and introduce the key notations in Sec.3.1. Then present the proposed MDAA framework, which incorporates ACs into pre-trained multi-modal encoders (Sec.3.2). Subsequently, we detail the AC adaptation in Sec.3.3 and introduce DLFM for updating process in Sec.3.4. An overview of MDAA is provided in Figure 2.

3.1 Problem Definition and Notations

To illustrate our method, we consider an audio-video classification task, which generalizes to other multi-modal scenarios without loss of generality. In MM-CTTA, the weight in pre-trained models \mathbf{W}_{Sr} is trained on a labeled source dataset $D_{\text{Sr}} \sim \{\mathbf{X}_{\text{Sr}}^a, \mathbf{X}_{\text{Sr}}^v, \mathbf{Y}_{\text{Sr}}\}$ in source domain Sr, where \mathbf{X}_{Sr}^a and \mathbf{X}_{Sr}^v represent the audio and video training data respectively. \mathbf{Y}_{Sr} represents the corresponding one-hot label set. During the adaptation phase, for each timestamp t in the target domain Tg, the model can only perform inference and update itself based on the unlabeled test dataset $D_{\text{Tg},t} \sim \{\mathbf{X}_{\text{Tg},t}^a, \mathbf{X}_{\text{Tg},t}^v\}$. The target domain varies with t and the whole adaptation process can be represented as $\mathbf{W}_{\text{Sr}} \rightarrow \mathbf{W}_{\text{Tg},1} \rightarrow \dots \rightarrow \mathbf{W}_{\text{Tg},t}$.

3.2 Source Model and Analytic Classifier Configuration

The multi-modal backbone follows a typical extraction–fusion architecture, where training data from different modalities are first processed by modality-specific feature encoders and subsequently fused through a fusion encoder. During this process, features from different encoders are projected into a unified higher-dimensional space to enhance representational capacity, and are then passed through a linear classifier to produce prediction labels, as illustrated in Figure 2.A. These linear classifiers are referred to as Analytic Classifiers (ACs). During the adaptation phase, both the feature encoders and the projection layers are kept frozen, while only the ACs are updated. Since features from different modalities are processed by ACs in a unified manner, we omit modality-specific distinctions for simplicity.

The weights \mathbf{W}_{Sr} for the ACs are optimized via ridge regression, initialized using a least squares objective, a strategy commonly employed in classification tasks [6, 28, 34, 35]. To address the issue of class imbalance, we reformulate the optimization objective as follows:

$$\underset{\mathbf{W}_{\text{Sr}}}{\operatorname{argmin}} \sum_{k=1}^{N_{\text{Sr}}} \omega_k \|\mathbf{y}_{\text{Sr},k} - \mathbf{x}_{\text{exf},k} \mathbf{W}_{\text{Sr}}\|_{\text{F}}^2 + \gamma \|\mathbf{W}_{\text{Sr}}\|_{\text{F}}^2, \quad (1)$$

where $\|\cdot\|_{\text{F}}$ indicates the Frobenius norm, γ is the regularization parameter and N_{Sr} is the samples size of D_{Sr} . ω_k , $\mathbf{x}_{\text{exf},k}$ and $\mathbf{y}_{\text{Sr},k}$ represents the weight, expanded feature vector and one-hot label of sample k in D_{Sr} , while the weight is further defined as

$$\omega_k = \frac{N_{\text{Sr}}}{N_{\text{C}} \times N_{c|k}}, \quad (2)$$

where N_{C} is the number of classes in D_{Sr} and $N_{c|k}$ is the number of samples in D_{Sr} from category c to which sample k belongs. Following the ridge regression solution, the solution to optimization

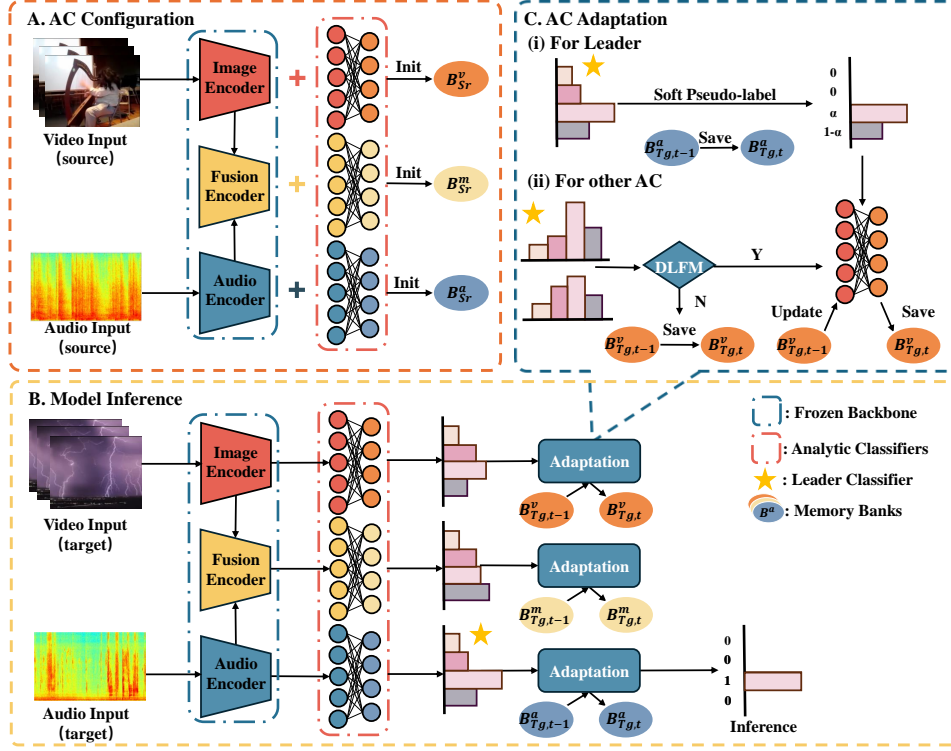


Figure 2: The overview of MDAA. (A) Construct Analytic Classifiers (ACs) and initialize the memory bank $B \sim \{P, Q\}$ to preserve knowledge from source datasets, using Eq. 4. (B) In the inference pipeline, the classifier with highest MAP is selected as *leader*. After adaptation, the model generates final predictions and updates the memory bank using Eq.9. (C) During adaptation, ACs determine whether to update by comparing with the soft pseudo-label from the *leader* through the Dynamic Late Fusion Mechanism (DLFM). The figure illustrates the process using the top 2 highest-probability labels.

problem is given as

$$\begin{aligned} \hat{\mathbf{W}}_{\text{Sr}} &= (\sum_{k=1}^{N_{\text{Sr}}} \tilde{\mathbf{x}}_{\text{exf},k}^{\top} \tilde{\mathbf{x}}_{\text{exf},k} + \gamma \mathbf{I})^{-1} \sum_{k=1}^{N_{\text{Sr}}} \tilde{\mathbf{x}}_{\text{exf},k}^{\top} \tilde{\mathbf{y}}_{\text{Sr},k} \\ &= (\tilde{\mathbf{X}}_{\text{exf},\text{Sr}}^{\top} \tilde{\mathbf{X}}_{\text{exf},\text{Sr}} + \gamma \mathbf{I})^{-1} \tilde{\mathbf{X}}_{\text{exf},\text{Sr}}^{\top} \tilde{\mathbf{Y}}_{\text{Sr}}, \end{aligned} \quad (3)$$

where $\tilde{\mathbf{x}}_{\text{exf},k} = \sqrt{\omega_k} \mathbf{x}_{\text{exf},k}$ and $\tilde{\mathbf{y}}_{\text{Sr},k} = \sqrt{\omega_k} \mathbf{y}_{\text{Sr},k}$. In addition to the classifier weights $\hat{\mathbf{W}}_{\text{Sr}}$, a memory bank B_{Sr} needs to be constructed during the training phase. Unlike other methods [2, 26, 30], our memory bank contains only two types of matrices, which can be represented as $B_{\text{Sr}} \sim \{P_{\text{Sr}}, Q_{\text{Sr}}\}$, where

$$\begin{cases} P_{\text{Sr}} = \tilde{\mathbf{X}}_{\text{exf},\text{Sr}}^{\top} \tilde{\mathbf{X}}_{\text{exf},\text{Sr}} + \gamma \mathbf{I}, \\ Q_{\text{Sr}} = \tilde{\mathbf{X}}_{\text{exf},\text{Sr}}^{\top} \tilde{\mathbf{Y}}_{\text{Sr}}. \end{cases} \quad (4)$$

Both P_{Sr} and Q_{Sr} are used to extract and preserve the learned knowledge from the source dataset, which cannot be accessed during adaptation. Therefore $\hat{\mathbf{W}}_{\text{Sr}}$ can be further rewritten as

$$\hat{\mathbf{W}}_{\text{Sr}} = P_{\text{Sr}}^{-1} Q_{\text{Sr}}. \quad (5)$$

3.3 Model Inference and Analytic Classifier Adaptation

During test time, MDAA determines the final prediction for each sample by selecting the output distribution with the highest maximum a posteriori (MAP) score across all ACs, as higher predictive

probabilities generally reflect greater confidence [1]. Subsequently, DLFM is employed to further filter the samples used for model updates, which will be elaborated upon in the following section.

Since ACL performs global optimization, it considers not only the currently selected input sample $\mathbf{X}_{\text{Tg},t}$ at timestamp t , but also all previously observed data, including $\mathbf{X}_{\text{Sr},k}$ and $\mathbf{X}_{\text{Tg},1:t-1}$. The corresponding optimization problem for the weight $\hat{\mathbf{W}}_{\text{Tg},t}$ is formulated as:

$$\begin{aligned} \operatorname{argmin}_{\mathbf{W}_{\text{Tg},t}} \sum_{k=1}^{N_{\text{Sr}}} \omega_k \|\mathbf{y}_{\text{Sr},k} - \mathbf{x}_{\text{exf},k} \mathbf{W}_{\text{Tg},t}\|_{\text{F}}^2 + \\ \|\tilde{\mathbf{Y}}_{\text{Tg},1:t} - \mathbf{X}_{\text{exf},1:t} \mathbf{W}_{\text{Tg},t}\|_{\text{F}}^2 + \gamma \|\mathbf{W}_{\text{Tg},t}\|_{\text{F}}^2, \end{aligned} \quad (6)$$

where $\tilde{\mathbf{Y}}$ denotes for soft pseudo-labels of filtered samples. We adopt soft labels for AC updates as they retain a richer representation of uncertainty compared to hard labels [12, 17]. For each filtered sample, we sort and choose its top- n class positions $C = c_1, c_2, \dots, c_n$ and assign weights $\alpha_1, \alpha_2, \dots, \alpha_n$ ($\sum_{i=1}^n \alpha_i = 1$). In this paper, we define the weights as $\alpha_i = \text{round}((n+1-i)/\sum_{i=1}^n i)$, and construct the soft pseudo-label accordingly as:

$$\bar{\mathbf{y}}_i = \begin{cases} \alpha_i & , i \in C \\ 0 & , \text{otherwise.} \end{cases} \quad (7)$$

Such reconstruction is proven to be useful, as shown in ablation study in subsection 4.3.

Due to the definition of TTA, all datasets (*i.e.*, $\mathbf{X}_{S_r,k}$ and $\mathbf{X}_{Tg,1:t-1}$) prior to timestamp t are not accessible when solving the optimization problem. However, with the aid of the memory bank $B_{Tg,t} \sim \{\mathbf{P}_{Tg,t}, \mathbf{Q}_{Tg,t}\}$, the solution can still be computed, as stated follow.

Theorem 1. The optimal solution to Formula 6 is given as

$$\hat{\mathbf{W}}_{Tg,t} = \mathbf{P}_{Tg,t}^{-1} \mathbf{Q}_{Tg,t}, \quad (8)$$

where

$$\begin{cases} \mathbf{P}_{Tg,t} = \mathbf{P}_{Tg,t-1} + \mathbf{X}_{\text{exf},t}^{\top} \mathbf{X}_{\text{exf},t}, \\ \mathbf{Q}_{Tg,t} = \mathbf{Q}_{Tg,t-1} + \mathbf{X}_{\text{exf},t}^{\top} \hat{\mathbf{Y}}_{Tg,t}. \end{cases} \quad (9)$$

Proof of **Theorem 1** is provided in Appendix D. It can be seen that, only features and labels that are accessible in phase t are involved in the adaptation, which fits the definition of TTA. Solution in Eq. 8 is the global optimal solution for all the samples that have appeared, therefore it is not affected by batch size and timestamp, thus solving the catastrophic forgetting at the root.

3.4 Dynamic Late Fusion Mechanism

Although AC-based adaptation effectively mitigates the forgetting issue, it is worth noting that employing the least squares loss as the objective function may be less robust to outliers compared to the cross-entropy loss. This vulnerability increases the risk of model collapse when adapting with corrupted modality inputs. This raises a critical question: **how can we reliably select trustworthy samples for updating each AC?**

To tackle this challenge, we propose a novel fusion strategy termed Dynamic Late Fusion Mechanism (DLFM). For each input sample, DLFM first identifies the AC yielding the highest MAP score, designating it as the *Leader*. During adaptation, each AC is updated independently based on its MAP score relative to the *Leader*. All possible relationships and update rules can be enumerated as four scenarios (see Figure 3).

(i). **Close Distributions:** When the MAP scores of the AC and the *Leader* are nearly identical and correspond to the same label, the AC remains unchanged to avoid reinforcing existing knowledge and causing class imbalance.

(ii). **Different Labels with Close Distributions:** If the MAP scores are similar but correspond to different labels, no update is made to avoid introducing potential errors due to uncertainty in the *Leader*'s prediction.

(iii). **Evenly Distributed Probabilities:** If both the AC and the *Leader* show evenly distributed probabilities with no clear preference, the AC is not updated to prevent adjustments based on uncertain predictions.

(iv). **Significant Difference:** If the *Leader*'s MAP is significantly higher than the AC's, the AC is updated to reflect the *Leader*'s confident prediction.

To summarize, cases (i),(ii) and (iii) all belong to a small gap between MAP scores of AC and *Leader*, while case (iv) belongs to a larger gap. Therefore, given a pre-defined threshold θ , Rules of DLFM can be noted as:

$$\begin{cases} \text{Accept,} & \text{Leader}_{\text{MAP}} - \text{AC}_{\text{MAP}} \geq \theta \\ \text{Reject,} & \text{otherwise.} \end{cases} \quad (10)$$

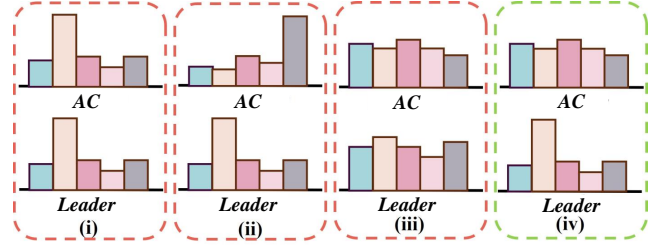


Figure 3: Four possible relationship between the probability distribution of *Leader* and compared AC. Only samples belong to case (iv) will be used to update AC.

DLFM leverages the complementary and consistent information across modalities to enhance adaptation. For complementarity, it selects the most reliable prediction—typically from an uncorrupted modality—as a pseudo label to update other classifiers, aligning corrupted inputs with reliable targets to handle domain shifts. For consistency, when all classifiers predict the same label, indicating high confidence and low likelihood of corruption, no update is performed to avoid unnecessary adaptation and prevent class imbalance. Since our recursive formulation already preserves prior knowledge, additional updates are unnecessary. By updating each classifier individually, DLFM maximizes modality-specific information while reducing reliability bias.

It is also important to note that in Eq. 6 we treat source data and target data separately, we adjust the category balance for the source dataset by assigning weights to each class. In contrast, it is challenging to apply this approach to the target dataset, as it is impossible to know the exact number of samples in each category within the target domain. However, with the help of the DLFM, category balance can still be maintained, as unimportant samples have been filtered out. Given that the weights added to the sample data are expected to average out to 1, the impact of each sample from both the source and target domains on the model can be considered equivalent.

4 EXPERIMENTS

In this section, we evaluate MDAA under two challenging settings which is detailed in Sec. 4.1. Sec. 4.2 compares MDAA with other SOTA methods through extensive experiments and Sec.4.3 conducts ablation studies on MDAA's components and computational efficiency. Implementation details are in Appendix B.

4.1 Benchmarks and Settings

To evaluate the model performance, we designed two tasks specifically for MM-CTTA. The first task named **Progressive single-modality corruption**, sequentially corrupts one modality while keeping the other clean, assessing the model's resistance to catastrophic forgetting. It follows an online setting, where the model processes one sample at a time, leading to an extreme long learning phase. The second task, called **interleaved modality corruption**, continually alternates corruption between the two modalities. While most methods perform poorly in the online setting due to severe catastrophic forgetting, this task uses a batch size of 64 during test time to emphasize assessing the model's ability to adapt to

Table 1: Comparison with SOTA methods on audio progressive single-modality corruption task in terms of classification Top-1 accuracy (%), using dataset Kinetics50-C and VGGSound-C in severity level 5. The best results for each domain are highlighted in bold. * means we revise the method from BN to LN for fair comparison.

Method	Type	Kinetics50-C							VGGSound-C						
		Gauss.	Traff.	Crowd	Rain	Thund.	Wind	Avg.	Gauss.	Traff.	Crowd	Rain	Thund.	Wind	Avg.
		$t \rightarrow$							$t \rightarrow$						
Source	-	73.97	65.17	67.88	70.24	68.00	70.44	69.28	37.29	21.24	16.89	21.81	27.36	25.66	25.04
TENT*	TTA	73.02	63.36	45.31	37.02	34.57	34.01	47.88	0.68	0.28	0.28	0.28	0.28	0.28	0.35
SAR	TTA	72.18	70.36	48.30	37.67	36.21	39.09	50.64	16.09	4.50	4.33	3.60	12.00	5.51	7.67
EATA	CTTA	73.91	65.29	68.24	70.51	68.28	70.48	69.45	40.39	31.99	31.91	32.38	39.24	33.95	34.98
MMTTA*	MM-TTA	17.03	1.99	1.99	1.99	1.99	1.99	4.50	0.41	0.33	0.33	0.33	0.33	0.33	0.34
READ	MM-TTA	65.65	49.34	46.45	44.94	44.45	43.72	49.09	18.73	8.52	8.01	5.90	8.30	4.82	9.05
READ+SRM	MM-CTTA	52.23	38.30	40.68	46.61	47.02	48.60	45.57	18.36	7.88	8.34	8.01	16.26	10.21	11.51
MDA	MM-CTTA	72.87	71.45	72.91	72.26	73.20	73.80	72.75	38.80	34.91	34.63	34.59	37.70	35.85	36.08
		$t \leftarrow$							$t \leftarrow$						
TENT*	TTA	43.27	42.96	43.81	60.19	69.17	70.17	54.93	0.30	0.30	0.30	0.30	0.30	0.39	0.32
SAR	TTA	41.81	27.94	24.41	40.47	42.90	70.36	41.32	14.91	4.56	4.61	3.72	12.44	5.94	7.70
EATA	CTTA	73.91	65.32	68.18	70.49	68.26	70.47	69.44	40.22	33.69	31.61	32.64	39.67	32.81	35.11
MMTTA*	MM-TTA	1.99	1.99	1.99	1.99	1.99	39.21	8.19	0.33	0.30	0.31	0.30	0.61	1.49	0.56
READ	MM-TTA	48.95	48.70	48.72	51.99	62.69	65.34	54.40	8.99	6.00	7.71	7.71	11.56	11.89	8.98
READ+SRM	MM-CTTA	48.59	47.39	46.48	41.11	38.01	51.90	45.58	18.50	7.93	8.36	7.96	16.28	10.11	11.53
MDA	MM-CTTA	74.86	72.63	72.87	72.26	73.4	72.02	73.01	38.95	35.46	34.66	34.70	37.31	35.20	36.05

Table 2: Comparison with SOTA methods on video progressive single-modality corruption task in terms of classification Top-1 accuracy (%), with dataset Kinetics50-C in severity level 5.

Method	Type	Gauss.	Shot.	Impul.	Defoc.	Glass.	Motion.	Zoom.	Snow	Frost	Fog	Bright.	Cont.	Elastic.	Pixel.	Jpeg	Avg.
				$t \rightarrow$													
Source	-	48.74	49.80	48.99	67.68	61.84	70.88	66.18	61.35	61.39	45.34	75.95	51.87	65.77	68.78	66.10	60.71
TENT*	TTA	16.23	2.07	2.03	2.08	2.06	2.03	2.03	2.03	2.03	2.03	2.03	2.03	2.03	2.03	2.03	2.98
SAR	TTA	38.36	35.97	34.51	44.40	48.86	50.77	47.53	43.59	35.81	42.54	52.11	35.44	50.20	40.15	50.73	43.40
EATA	CTTA	48.80	49.82	49.03	67.66	61.98	70.84	66.16	61.64	61.54	45.40	75.99	51.95	65.88	68.71	66.08	60.77
MMTTA*	MM-TTA	14.31	2.64	2.03	2.03	2.03	2.03	2.03	2.03	2.03	2.03	2.03	2.03	2.03	2.03	2.03	2.89
READ	MM-TTA	12.76	2.03	2.02	3.27	2.60	2.64	2.64	2.50	2.39	2.42	2.44	2.40	2.42	2.40	2.41	3.16
READ+SRM	MM-CTTA	41.90	42.29	42.27	54.78	54.37	58.21	56.70	53.70	52.68	46.12	61.97	45.16	58.63	55.32	54.54	52.68
MDA	MM-CTTA	54.89	55.25	55.32	63.89	62.49	67.26	65.86	64.32	65.31	61.86	73.20	61.60	67.83	69.22	68.69	63.80
		$t \leftarrow$															
TENT*	TTA	2.03	2.03	2.03	2.03	2.03	2.03	2.03	2.03	2.03	2.03	2.03	2.03	2.10	3.47	53.26	5.55
SAR	TTA	34.75	35.08	35.89	42.70	45.99	49.43	50.12	44.08	42.42	40.02	57.54	35.56	48.86	57.22	66.26	45.73
EATA	CTTA	48.81	49.79	49.02	67.71	61.96	70.88	66.17	61.56	61.51	45.38	75.96	51.90	65.90	68.76	66.09	60.76
MMTTA*	MM-TTA	1.99	1.99	1.99	1.99	1.99	1.99	1.99	1.99	1.99	1.99	1.99	1.99	1.99	1.99	23.88	3.45
READ	MM-TTA	2.03	2.03	2.03	2.03	2.03	2.03	2.03	2.03	2.09	2.03	2.22	2.04	2.43	3.65	24.34	3.67
READ+SRM	MM-CTTA	41.91	42.42	42.46	54.97	54.32	58.30	56.83	53.66	52.93	46.03	62.05	45.00	58.69	55.20	54.60	53.19
MDA	MM-CTTA	67.32	67.48	67.76	68.98	67.60	69.59	68.49	66.46	66.18	63.14	72.87	59.33	66.59	67.64	65.25	66.98

Table 3: Comparison with SOTA methods on video progressive single-modality corruption task in terms of classification Top-1 accuracy (%), with dataset VGGSound-C in severity level 5.

Method	Type	Gauss.	Shot.	Impul.	Defoc.	Glass.	Motion.	Zoom.	Snow	Frost	Fog	Bright.	Cont.	Elastic.	Pixel.	Jpeg	Avg.
				$t \rightarrow$													
Source	-	53.02	52.90	52.98	57.20	57.38	58.37	57.48	56.40	56.46	55.41	59.16	53.73	57.22	56.44	57.33	56.10
TENT*	TTA	51.48	50.70	50.87	51.15	50.90	51.09	50.82	50.65	50.75	50.73	50.73	50.58	50.70	50.73	50.70	50.84
SAR	TTA	43.12	38.99	37.77	42.43	43.84	43.61	43.79	42.13	41.26	42.83	43.84	39.34	42.75	43.49	40.38	41.97
EATA	CTTA	53.57	53.70	53.57	57.00	57.29	58.46	57.77	56.24	56.57	55.45	59.06	54.13	58.24	57.22	57.38	56.38
MMTTA*	MM-TTA	0.46	0.34	0.34	0.34	0.34	0.34	0.34	0.34	0.34	0.34	0.34	0.34	0.34	0.34	0.34	0.35
READ	MM-TTA	33.12	10.41	4.05	0.77	0.37	0.35	0.32	0.29	0.29	0.29	0.29	0.29	0.29	0.29	0.29	3.45
READ+SRM	MM-CTTA	41.33	41.37	41.32	45.50	45.68	47.18	46.61	44.66	44.88	42.97	47.07	40.01	46.18	45.41	45.24	44.36
MDA	MM-CTTA	55.13	55.29	55.30	56.91	57.20	57.78	57.32	56.52	56.25	56.14	58.11	55.32	57.06	56.27	57.39	56.53
		$t \leftarrow$															
TENT*	TTA	52.68	52.74	52.49	53.45	53.45	53.50	53.10	53.35	53.67	52.83	55.86	51.82	56.81	57.46	57.43	54.04
SAR	TTA	40.31	39.24	38.33	41.53	41.36	44.43	43.59	42.46	41.11	41.52	42.24	38.97	43.49	40.97	46.22	41.72
EATA	CTTA	53.63	53.60	53.61	57.06	57.27	58.35	57.83	56.22	56.74	55.73	59.16	54.09	58.19	57.27	57.35	56.41
MMTTA*	MM-TTA	0.34	0.34	0.34	0.34	0.34	0.34	0.34	0.34	0.34	0.34	0.34	0.34	0.34	0.34	8.32	0.87
READ	MM-TTA	13.26	13.39	13.38	13.66	13.72	13.91	13.92	14.25	14.84	18.15	20.68	22.85	29.46	40.99	50.38	20.46
READ+SRM	MM-CTTA	41.46	41.25	41.41	45.77	45.95	47.17	46.85	44.73	45.03	43.37	46.90	39.93	46.32	45.46	45.18	44.45
MDA	MM-CTTA	55.30	55.38	55.25	56.90	57.19	57.79	57.32	56.50	56.31	56.22	58.13	55.28	57.07	56.30	57.47	56.56

Table 4: Comparison with SOTA methods on interleaved modality corruption task in terms of classification Top-1 accuracy (%), with dataset Kinetics50-C in severity level 5. A-C and V-C indicates the corrupted modality in current phase.

Method	V-C		A-C	V-C		A-C	V-C		A-C	V-C			A-C	V-C		A-C	V-C		Avg.			
	Gauss.	Shot.	Gauss.	Impul.	Defoc.	Traff.	Glass.	Motion.	Crowd	Zoom.	Snow	Frost	Rain	Fog	Bright.	Thund.	Cont.	Elastic.	Wind	Pixel.	Jpeg	
Source	48.71	49.98	74.03	48.98	67.69	67.89	61.82	70.92	70.29	66.14	61.36	61.35	68.02	45.34	75.94	65.20	51.82	65.84	70.38	68.73	66.11	63.17
TENT*	48.77	48.34	74.11	46.38	62.83	67.22	62.30	68.35	69.32	64.61	54.64	57.36	66.32	46.22	63.95	37.12	38.87	42.77	40.62	10.13	5.40	51.22
SAR	48.65	49.81	74.15	48.53	66.87	65.68	62.56	70.67	68.00	66.45	58.80	60.42	69.96	47.69	75.19	67.89	50.96	65.54	70.03	66.77	63.67	62.78
EATA	48.81	49.70	74.07	48.96	67.75	65.35	61.96	70.95	67.98	66.05	61.60	61.49	70.40	45.29	76.11	68.13	51.85	65.98	70.51	68.80	66.15	63.23
MMTTA*	48.63	49.20	56.24	47.79	47.52	4.76	42.96	29.87	1.96	4.13	2.27	1.96	1.96	1.96	1.92	2.03	1.96	1.92	1.96	1.92	1.99	16.90
READ	51.18	53.62	73.88	54.73	68.67	67.95	67.07	70.14	68.84	67.62	62.68	64.90	68.24	59.46	71.43	68.16	52.60	66.35	66.18	62.85	63.35	64.28
READ+SRM	46.18	45.39	55.52	44.25	56.45	44.43	55.42	59.41	49.61	57.63	54.45	53.65	50.92	50.60	62.39	52.52	45.93	59.55	52.69	55.92	56.06	52.81
MDAA	55.04	55.91	73.64	55.89	63.78	73.12	63.54	67.62	74.90	67.00	65.60	67.21	75.44	64.89	72.69	76.94	65.45	69.21	76.95	70.94	71.16	67.95
Source	48.73	49.75	74.02	48.99	67.61	65.21	61.93	70.87	67.87	66.17	61.36	61.43	70.27	45.32	75.88	67.97	51.84	65.74	70.47	68.74	66.10	63.16
TENT*	6.72	10.03	52.92	23.89	53.44	63.96	60.40	64.98	67.75	62.93	60.28	61.20	67.26	52.50	71.88	58.44	51.24	67.56	70.84	68.87	66.41	55.40
SAR	47.97	48.73	72.21	48.46	66.39	66.75	63.69	70.28	68.00	66.33	59.24	59.85	70.17	46.42	75.52	67.59	51.12	65.23	70.24	68.31	66.18	62.79
EATA	48.76	49.76	73.89	48.86	67.75	65.20	61.89	70.67	68.28	66.16	61.64	61.44	70.33	45.57	75.96	68.30	51.88	65.87	70.51	68.59	65.98	63.20
MMTTA*	1.96	1.96	2.00	1.96	1.96	2.00	2.00	2.03	1.96	2.03	1.96	2.00	1.96	2.52	18.31	4.88	43.11	49.71	62.28	55.69	60.04	15.35
READ	51.49	52.29	71.09	50.70	62.44	63.72	65.01	66.42	66.39	64.86	60.97	64.44	67.85	62.48	74.68	72.12	54.12	69.15	70.27	69.74	68.37	64.22
READ+SRM	44.57	44.24	55.61	44.36	56.04	44.20	55.60	59.01	50.48	57.75	54.41	53.47	50.80	50.95	62.64	52.76	46.44	60.00	53.65	56.84	58.81	52.98
MDAA	70.44	70.21	77.35	70.12	72.13	76.56	70.05	72.44	76.07	71.46	68.94	68.72	75.92	66.51	73.32	75.10	61.78	68.05	73.52	68.56	64.91	71.06

Table 5: Comparison with SOTA methods on interleaved modality corruption task in terms of classification Top-1 accuracy (%), with dataset VGGSound-C in severity level 5.

Method	V-C		A-C	V-C		A-C	V-C		A-C	V-C			A-C	V-C		A-C	V-C		Avg.			
	Gauss.	Shot.	Gauss.	Impul.	Defoc.	Traff.	Glass.	Motion.	Crowd	Zoom.	Snow	Frost	Rain	Fog	Bright.	Thund.	Cont.	Elastic.	Wind	Pixel.	Jpeg	
Source	53.05	52.91	37.32	52.98	57.19	21.24	57.37	58.37	16.89	57.45	56.37	56.47	21.82	55.41	59.19	27.37	53.75	57.19	25.66	56.44	57.33	47.23
TENT*	53.19	52.80	3.43	50.52	53.15	0.65	51.83	53.10	0.60	52.64	50.91	51.89	0.67	51.15	51.73	2.13	48.68	50.76	0.79	50.38	50.22	37.20
SAR	53.16	53.33	34.26	53.17	56.94	11.27	57.14	58.29	9.30	57.65	56.11	56.78	13.36	55.94	57.87	17.95	53.13	56.51	20.46	55.30	55.79	44.94
EATA	53.63	53.70	40.51	53.59	57.21	30.81	57.45	58.49	29.80	57.85	56.37	56.85	30.55	56.72	59.13	37.29	54.31	58.27	32.58	57.28	57.55	50.00
MMTTA*	8.27	0.34	0.34	0.34	0.34	0.34	0.34	0.34	0.34	0.34	0.34	0.34	0.34	0.34	0.34	0.34	0.34	0.34	0.34	0.34	0.34	0.72
READ	53.78	53.91	39.83	54.17	57.81	26.00	58.14	59.42	21.63	59.03	57.38	58.29	22.79	57.71	59.32	26.07	55.46	58.36	18.29	57.36	57.63	48.21
READ+SRM	42.34	41.70	22.88	41.73	45.39	10.93	45.62	46.75	11.23	46.28	45.00	44.82	10.92	42.59	47.43	19.22	40.47	46.43	12.57	45.02	45.39	35.94
MDAA	55.09	55.31	38.60	55.31	56.89	34.83	57.20	57.69	34.65	57.35	56.47	56.27	34.28	56.17	58.05	36.86	55.33	57.00	35.53	56.28	57.35	50.60
Source	53.01	52.88	37.31	52.97	57.20	21.25	57.42	58.41	16.89	57.49	56.37	56.49	21.81	55.43	59.16	27.37	53.74	57.19	25.66	56.42	57.29	47.23
TENT*	24.80	42.44	1.65	49.78	51.65	0.32	51.64	51.52	0.34	51.35	50.51	50.89	0.43	51.27	52.07	1.14	51.14	54.94	1.64	56.50	56.92	35.85
SAR	51.90	51.78	25.90	51.30	54.73	5.11	54.82	56.52	7.82	56.31	54.63	55.49	13.44	55.12	57.59	15.07	53.57	56.92	15.04	56.53	57.30	43.19
EATA	53.77	53.65	40.39	53.61	57.17	30.49	57.36	58.59	30.16	57.82	56.21	56.64	31.22	56.77	59.24	37.44	54.30	58.18	33.01	57.46	57.53	50.05
MMTTA*	0.34	0.34	0.34	0.34	0.34	0.34	0.34	0.34	0.34	0.34	0.34	0.34	0.34	0.34	0.34	0.34	0.34	0.34	0.34	0.34	0.34	0.72
READ	54.35	54.56	25.03	54.38	57.99	17.67	57.76	58.74	20.57	58.66	56.91	57.58	20.81	58.04	59.10	33.82	55.54	58.13	32.75	57.80	58.34	48.03
READ+SRM	41.84	41.72	21.72	41.78	45.17	10.47	45.62	46.73	11.84	46.34	44.98	44.83	10.98	42.69	47.49	19.50	40.59	46.53	12.48	44.97	45.96	35.92
MDAA	55.30	55.41	38.64	55.29	56.91	35.40	57.14	57.81	34.85	57.34	56.48	56.29	34.52	56.23	58.24	37.22	55.31	57.13	35.12	56.30	57.47	50.69

dynamic reliability biases. We utilize two datasets for both tasks: Kinetics50 [13] and VGGSound [4]. Following [27], we construct their corrupted type named Kinetics50-C and VGGSound-C, each dataset includes 15 types of video corruptions and 6 audio corruptions at the largest severity (level 5).

4.2 Performance Comparison

In this section, we reproduce various TTA methods under the MM-CTTA setting. These include typical TTA methods (TENT [23], SAR [19]), CTTA methods (EATA [18]), and MM-TTA methods (MMTTA [21], READ [26]). Additionally, we introduce an MM-CTTA variant, READ+SRM, which integrates READ with the stochastic restoration mechanism (SRM) from CoTTA [24]. To ensure fairness, all methods use the same pre-trained model CAV-MAE [9] as the multi-modal encoder. For methods that update BN layers, we instead update LN layers to align with the ViT structure of encoder. We also evaluate the source model, a baseline trained only on the source dataset and kept frozen during testing.

The performances of various methods on **progressive single-modality corruption** are summarized in Tables 1, 2, and 3. Table 1 reports results on audio corruption, while Tables 2 and 3 focus on video corruption. Notably, most comparison methods collapse on

VGGSound-C, performing worse than source models. In contrast, EATA achieves better results by limiting parameter updates, enabling more stable adaptation. MDAA outperforms prior methods by 3.00%-3.57% (audio) and 3.03%-6.22% (video) on Kinetics50-C, and by 0.94%-1.10% (audio) and 0.13%-0.18% (video) on VGGSound-C, on average. While MDAA exhibits suboptimal performance in scenarios where data corruption minimally impacts source model performance—attributable to its reduced parameter space for adaptation compared to baselines—it nevertheless demonstrates superior overall adaptability. MDAA consistently retains its advantage in later stages of the tasks, demonstrating superior robustness against catastrophic forgetting in MM-CTTA.

The comparison results of **interleaved modality corruption** tasks are shown in Table 4 and 5. In this task, EATA, which is more good at memorization, is not dominant in the task of highlighting reliability bias. READ, which is specifically designed to address intra-modal reliability bias, demonstrates strong performance in this area. However, its effectiveness is limited to video corruption in MM-CTTA, as performance drops significantly during audio corruption. In contrast, MDAA is well-adapted to the corruption of different modalities, outperforming READ by 2.39%-6.84% and EATA by 0.60%-7.28% on average across Kinetics50-C and VGGSound-C.

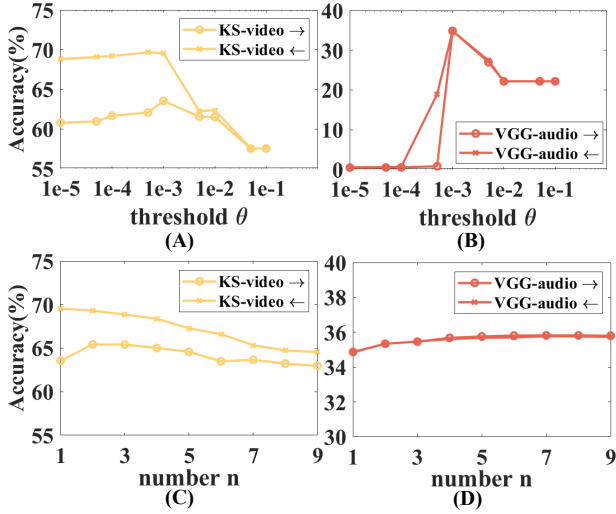


Figure 4: (A-B) Comparison of different thresholds θ . (C-D) Comparison of reconstructed pseudo-labels with varying category numbers.

4.3 Ablation Study

All studies in this section use the video-corrupted Kinetics50-C (KS-video) and audio-corrupted VGGSound-C (VGG-audio) datasets at severity level 5 with a batch size of 64.

Component analysis. To verify the effectiveness of each MDAA component, we adopt an ablation study *w.r.t* three components as shown in Table 6. As observed, due to the vulnerability of least square loss, the model using only ACs underperforms, with an average accuracy 0.5%-0.57% lower than READ (using cross-entropy loss) on KS-video. The model even collapses on VGG-audio, with an average accuracy of 0.47%-0.56%. The introduction of DLFM consistently improves model performance across all types of corruption, achieving the gains of 1.73%-7.52% on KS-video and 33.74%-33.90% on VGG-audio. Soft labeling introduces a small amount of uncertainty compared to hard labeling, it effectively alleviates the negative impact caused by incorrect pseudo labels during TTA. Although such uncertainty may lead to slightly lower performance in some tasks where corruptions in these tasks caused little effect on the model classification, soft labeling represents a favorable trade-off, particularly when dealing with highly complex datasets such as VGGSound. Furthermore, combining DLFM with soft labels yields the best overall performance.

Reliable selection threshold. To examine the effect of the threshold θ on the DLFM, we plot the model’s performance with θ of from $1e-5$ to $1e-1$ in Figure 4(A-B). The performance of the model on both datasets exhibits an increasing and then decreasing trend. When θ is close to 0, the ACs are updated for nearly every sample, introducing more error. Conversely, when θ increases too much, the ACs do not learn from new inputs since no samples can pass through the DLFM, leading to a decline in performance. Therefore, value of θ should not be too small, otherwise the model will not be able to filter out the update samples with low execution. For both datasets in the experiment, a reasonable value of θ is around $1e-3$.

Table 6: Ablation studies on different component combinations. Grey denotes the default setting.

Method	KS-video		VGG-audio	
	\rightarrow	\leftarrow	\rightarrow	\leftarrow
READ	62.32	62.59	23.93	22.39
MDAA (ACs+Hard)	61.82	62.02	0.47	0.56
MDAA (ACs+Soft)	61.33	67.47	32.50	33.00
MDAA (ACs+DLFM+Hard)	63.55	69.54	34.87	34.85
MDAA (ACs+DLFM+Soft)	65.43	69.30	35.82	35.77

Table 7: Comparison of runtime and VRAM usage.

Method	KS-video		VGG-audio	
	time(s)	memory(MB)	time(s)	memory(MB)
TENT*	1085	37620	2571	37622
SAR	2149	37620	4823	39220
EATA	889	67286	2313	38300
MMTTA*	2574	71732	5966	68840
READ	1174	9176	2611	9178
MDAA	1024	8784	1682	8750

Soft label reconstruction. Figure 4(C-D) shows the model results with n ranging from 1 to 9. While using soft labels inevitably introduces error, there are cases such as KS-video \rightarrow where one-hot labels may outperform soft labels. However, using soft pseudo-labels remains beneficial as datasets become larger and more complex. The choice of n needs to be moderate, as larger datasets with more categories tend to require larger n , while more error is likely to be introduced as n increases. In this work, we determine to use top 2 and 7 classes for label reconstruction in Kinetics50-C and VGGSound-C respectively.

Runtime and VRAM usage. To demonstrate MDAA’s practicality, we compare its runtime and VRAM usage against various methods in Table 7. MDAA achieves superior efficiency with lower memory overhead and faster execution, thanks to its unique design. Unlike other methods, MDAA eliminates backpropagation, reducing gradient computation and optimizer storage costs. The primary computational cost of MDAA lies in matrix inversion, with a time complexity of $O(\varphi^3)$, where φ is the expanded feature dimension, fixed at 8000 in our experiments.

5 CONCLUSION

MM-CTTA shows great potential in real-world scenarios, as it enables pre-trained models to handle multi-modal inputs and adapt to continuously changing target domains. However, it also suffers from critical challenges such as reliability bias and catastrophic forgetting. To tackle these issues, we propose a new paradigm, MDAA, which introduces analytic learning into TTA. Instead of simply adapting the model to the target domain, MDAA integrates the target domain into source domain, and thus prevent network from forgetting. With the help of DLFM, model is able to dynamically and comprehensively process the information provided by each modality and use reliable samples to update. Moreover, compared to most SOTA TTA methods, MDAA achieves faster computational times and lower memory usage, highlighting its robust applicability in real-time deployment. In the future, we will try to adapt this method to more modalities to solve more challenging tasks.

ACKNOWLEDGMENTS

This research was supported by the National Natural Science Foundation of China (Grant No. 62306117), the Guangzhou Basic and Applied Basic Research Foundation (2024A04J3681), and GJYC program of Guangzhou (2024D03J0005).

REFERENCES

- [1] Malik Boudiaf, Romain Mueller, Ismail Ben Ayed, and Luca Bertinetto. 2022. Parameter-free online test-time adaptation. In *Proceedings of the IEEE/CVF Conference on Computer Vision and Pattern Recognition*. 8344–8353.
- [2] Haozhi Cao, Yuecong Xu, Jianfei Yang, Pengyu Yin, Shenghai Yuan, and Lihua Xie. 2023. Multi-modal continual test-time adaptation for 3d semantic segmentation. In *Proceedings of the IEEE/CVF International Conference on Computer Vision*. 18809–18819.
- [3] Chaoqi Chen, Weiping Xie, Wenbing Huang, Yu Rong, Xinghao Ding, Yue Huang, Tingyang Xu, and Junzhou Huang. 2019. Progressive feature alignment for unsupervised domain adaptation. In *Proceedings of the IEEE/CVF conference on computer vision and pattern recognition*. 627–636.
- [4] Honglie Chen, Weidi Xie, Andrea Vedaldi, and Andrew Zisserman. 2020. Vg-sound: A large-scale audio-visual dataset. In *ICASSP 2020-2020 IEEE International Conference on Acoustics, Speech and Signal Processing (ICASSP)*. IEEE, 721–725.
- [5] Alexey Dosovitskiy, Lucas Beyer, Alexander Kolesnikov, Dirk Weissenborn, Xi-aohua Zhai, Thomas Unterthiner, Mostafa Dehghani, Matthias Minderer, Georg Heigold, Sylvain Gelly, et al. 2020. An image is worth 16x16 words: Transformers for image recognition at scale. In *International Conference on Learning Representations*.
- [6] Di Fang, Yinan Zhu, Runze Fang, Cen Chen, Ziqian Zeng, and Huiping Zhuang. 2024. AIR: Analytic Imbalance Rectifier for Continual Learning. *arXiv preprint arXiv:2408.10349* (2024).
- [7] Jin Gao, Jialing Zhang, Xihui Liu, Trevor Darrell, Evan Shelhamer, and Dequan Wang. 2023. Back to the source: Diffusion-driven adaptation to test-time corruption. In *Proceedings of the IEEE/CVF Conference on Computer Vision and Pattern Recognition*. 11786–11796.
- [8] Taesik Gong, Jongheon Jeong, Taewon Kim, Yewon Kim, Jinwoo Shin, and Sung-Ju Lee. 2022. Note: Robust continual test-time adaptation against temporal correlation. *Advances in Neural Information Processing Systems* 35 (2022), 27253–27266.
- [9] Yuan Gong, Andrew Rouditchenko, Alexander H Liu, David Harwath, Leonid Karlinsky, Hilde Kuehne, and James Glass. 2022. Contrastive audio-visual masked autoencoder. *arXiv preprint arXiv:2210.07839* (2022).
- [10] Ping Guo and Michael R Lyu. 2004. A pseudoinverse learning algorithm for feedforward neural networks with stacked generalization applications to software reliability growth data. *Neurocomputing* 56 (2004), 101–121.
- [11] Zirun Guo and Tao Jin. 2025. Smoothing the shift: Towards stable test-time adaptation under complex multimodal noises. *arXiv preprint arXiv:2503.02616* (2025).
- [12] Geoffrey Hinton, Oriol Vinyals, and Jeff Dean. 2015. Distilling the Knowledge in a Neural Network. *stat* 1050 (2015), 9.
- [13] Will Kay, Joao Carreira, Karen Simonyan, Brian Zhang, Chloe Hillier, Sudheendra Vijayanarasimhan, Fabio Viola, Tim Green, Trevor Back, Paul Natsev, et al. 2017. The kinetics human action video dataset. *arXiv preprint arXiv:1705.06950* (2017).
- [14] Jixiang Lei and Franz Pernkopf. 2024. Two-Level Test-Time Adaptation in Multimodal Learning. In *ICML 2024 Workshop on Foundation Models in the Wild*.
- [15] Jian Liang, Ran He, and Tieniu Tan. 2024. A comprehensive survey on test-time adaptation under distribution shifts. *International Journal of Computer Vision* (2024), 1–34.
- [16] Michael McCloskey and Neal J Cohen. 1989. Catastrophic interference in connectionist networks: The sequential learning problem. In *Psychology of learning and motivation*. Vol. 24. Elsevier, 109–165.
- [17] Rafael Müller, Simon Kornblith, and Geoffrey E Hinton. 2019. When does label smoothing help? *Advances in neural information processing systems* 32 (2019).
- [18] Shuaicheng Niu, Jiaxiang Wu, Yifan Zhang, Yaofu Chen, Shijian Zheng, Peilin Zhao, and Mingkui Tan. 2022. Efficient test-time model adaptation without forgetting. In *International conference on machine learning*. PMLR, 16888–16905.
- [19] Shuaicheng Niu, Jiaxiang Wu, Yifan Zhang, Zhiquan Wen, Yaofu Chen, Peilin Zhao, and Mingkui Tan. 2023. Towards Stable Test-time Adaptation in Dynamic Wild World. In *The Eleventh International Conference on Learning Representations*.
- [20] Alec Radford, Jong Wook Kim, Chris Hallacy, Aditya Ramesh, Gabriel Goh, Sandhini Agarwal, Girish Sastry, Amanda Askell, Pamela Mishkin, Jack Clark, et al. 2021. Learning transferable visual models from natural language supervision. In *International conference on machine learning*. PMLR, 8748–8763.
- [21] Inkyu Shin, Yi-Hsuan Tsai, Bingbing Zhuang, Samuel Schuster, Buyu Liu, Sparsh Garg, In So Kweon, and Kuk-Jin Yoon. 2022. Mm-tta: multi-modal test-time adaptation for 3d semantic segmentation. In *Proceedings of the IEEE/CVF Conference on Computer Vision and Pattern Recognition*. 16928–16937.
- [22] A Vaswani. 2017. Attention is all you need. *Advances in Neural Information Processing Systems* (2017).
- [23] Dequan Wang, Evan Shelhamer, Shaoteng Liu, Bruno Olshausen, and Trevor Darrell. 2021. Tent: Fully Test-Time Adaptation by Entropy Minimization. In *International Conference on Learning Representations*.
- [24] Qin Wang, Olga Fink, Luc Van Gool, and Dengxin Dai. 2022. Continual test-time domain adaptation. In *Proceedings of the IEEE/CVF Conference on Computer Vision and Pattern Recognition*. 7201–7211.
- [25] Weiyao Wang, Du Tran, and Matt Feiszli. 2020. What makes training multi-modal classification networks hard?. In *Proceedings of the IEEE/CVF conference on computer vision and pattern recognition*. 12695–12705.
- [26] Baochen Xiong, Xiaoshan Yang, Yaguang Song, Yaowei Wang, and Changsheng Xu. 2024. Modality-Collaborative Test-Time Adaptation for Action Recognition. In *Proceedings of the IEEE/CVF Conference on Computer Vision and Pattern Recognition*. 26732–26741.
- [27] Mouxing Yang, Yunfan Li, Changqing Zhang, Peng Hu, and Xi Peng. 2024. Test-time Adaptation against Multi-modal Reliability Bias. In *The Twelfth International Conference on Learning Representations*.
- [28] Shuang-Hong Yang and Bao-Gang Hu. 2008. A stagewise least square loss function for classification. In *Proceedings of the 2008 SIAM International Conference on Data Mining*. SIAM, 120–131.
- [29] Xu Zhang, Felix Xinnan Yu, Shih-Fu Chang, and Shengjin Wang. 2015. Deep transfer network: Unsupervised domain adaptation. *arXiv preprint arXiv:1503.00591* (2015).
- [30] Yifan Zhang, Xue Wang, Kexin Jin, Kun Yuan, Zhang Zhang, Liang Wang, Rong Jin, and Tieniu Tan. 2023. Adanpc: Exploring non-parametric classifier for test-time adaptation. In *International Conference on Machine Learning*. PMLR, 41647–41676.
- [31] Yusheng Zhao, Junyu Luo, Xiao Luo, Jinsheng Huang, Jingyang Yuan, Zhiping Xiao, and Ming Zhang. 2025. Attention Bootstrapping for Multi-Modal Test-Time Adaptation. In *Proceedings of the AAAI Conference on Artificial Intelligence*, Vol. 39. 22849–22857.
- [32] Zhi Zhou, Lan-Zhe Guo, Lin-Han Jia, Dingchu Zhang, and Yu-Feng Li. 2023. ODS: Test-Time Adaptation in the Presence of Open-World Data Shift. In *Proceedings of the 40th International Conference on Machine Learning (Proceedings of Machine Learning Research, Vol. 202)*, Andreas Krause, Emma Brunskill, Kyunghyun Cho, Barbara Engelhardt, Sivan Sabato, and Jonathan Scarlett (Eds.). PMLR, 42574–42588.
- [33] Huiping Zhuang, Zhiping Lin, and Kar-Ann Toh. 2021. Blockwise recursive Moore–Penrose inverse for network learning. *IEEE Transactions on Systems, Man, and Cybernetics: Systems* 52, 5 (2021), 3237–3250.
- [34] Huiping Zhuang, Zhenyu Weng, Run He, Zhiping Lin, and Ziqian Zeng. 2023. Gkeal: Gaussian kernel embedded analytic learning for few-shot class incremental task. In *Proceedings of the IEEE/CVF Conference on Computer Vision and Pattern Recognition*. 7746–7755.
- [35] Huiping Zhuang, Zhenyu Weng, Hongxin Wei, Renchunzi Xie, Kar-Ann Toh, and Zhiping Lin. 2022. ACL: Analytic class-incremental learning with absolute memorization and privacy protection. *Advances in Neural Information Processing Systems* 35 (2022), 11602–11614.

A PSEUDO-CODE FOR MDAA

The pseudo-code of MDAA is shown in Algorithm 1. For the pre-trained models, we integrate an individual AC for each network block, using the source dataset to initialize the classifiers as well as the memory bank. During the inference and adaptation periods, the model reconstructs the output labels for each sample using the soft pseudo-label and determines which ACs need to be updated through the DLFM.

Algorithm 1 Multi-modality Dynamic Analytic Adaptor (MDAA)

Require: Source datasets $D_{Sr} \sim \{X_{Sr}^a, X_{Sr}^v, Y_{Sr}\}$ and target datasets $D_{Tg,t} \sim \{X_{Tg,t}^a, X_{Tg,t}^v\}$, pre-trained network Φ_{Sr} .

1. Training phase:
 - (1) integrate AC for each network block;
 - (2) Determine the parameters of each AC using D_{Sr} through Eq. 3;
- (3) Initialize the memory bank B_S through Eq. 4.

2. Inference and Adaptation phase:

for Samples in each batch **do**

- (1) Calculate the output *Leader* of each classifier and choose *Leader* classifier;
- (2) Reconstruct *Leader*'s label as soft pseudo-label;

for Each AC **do**

Determine whether to update using DLFM (Eq. 10);

if needs to be updated **then**

Update parameters through Eq. 8;

Update memory bank through Eq. 9.

end if

end for

end for

B BENCHMARKS, BACKBONE AND IMPLEMENTATION DETAILS

B.1 Details about the Benchmarks

ALL experiments are conducted on the two popular multi-modal datasets Kinetics [13] and VGGSound [4]. [27] further provides their corrupted visual and audio modality for TTA tasks.

Kinetics50 is a subset of the Kinetics dataset [13], consisting of 50 randomly selected classes [27]. It primarily includes videos that focus on human motion-related activities, with each clip lasting approximately 10 seconds and labeled with a single action class. All videos are sourced from YouTube. The Kinetics50 dataset comprises 29,204 visual-audio pairs for training and 2,466 pairs for testing, with the video modality playing a more prominent role in modality pairing.

VGGSound is a large-scale audio-visual dataset containing short audio clips extracted from YouTube videos [4], covering 309 distinct everyday audio events. Each clip has a fixed duration of 10 seconds. For this study, we utilize the 157,602 pairs for training and 14,046 pairs for testing. Compared to Kinetics50, VGGSound includes a wider range of categories, introducing additional complexity to the classification task.

Both datasets' visual and audio modalities were extracted following the method described in [9]. To systematically explore the

distributional shifts across modalities, various corruption types were applied to both visual and audio components. Following [27], 15 corruption types were introduced for the visual modality, each with five levels of severity for comprehensive evaluation. These corruptions include "gaussian noise", "shot noise", "impulse noise", "defocus blur", "glass blur", "motion blur", "zoom blur", "snow", "frost", "fog", "brightness", "contrast", "elastic transform", "pixelate", and "jpeg compression". Similarly, the audio modality was subjected to 6 different corruptions: "gaussian noise", "traffic noise", "crowd noise", "rain", "thunder", and "wind". The corrupted versions of these benchmarks are referred to as Kinetics50-C and VGGSound-C, respectively. Visualizations of sample corrupted video frames and audio spectrograms are provided in Figure 5 and Figure 6.

B.2 CAV-MAE Backbone

CAV-MAE is employed as the pre-trained models for MM-CTTA in this paper. Its architecture consists of 11 Transformer blocks (known as feature encoder networks) dedicated to modality-specific feature extraction, followed by an additional Transformer block (known as fusion network) responsible for cross modal fusion. For the video input, 10 frames are sampled from each clip, from which a single frame is randomly selected and fed into the Transformer encoder for the visual modality. In the case of the audio input, the original 10-second audio waveform is transformed into a 2D spectrogram before being processed by the Transformer encoder for the audio modality [8].

Table 8: Ablation studies on parameter γ .

γ	KS-video		VGG-audio	
	→	←	→	←
1e-3	2.10	2.08	0.51	0.47
1e-2	2.03	2.12	0.31	0.39
1e-1	64.87	69.03	0.32	0.37
1e0	65.43	69.30	0.36	0.40
1e1	65.27	69.23	35.82	35.77
1e2	65.29	68.95	35.78	35.76
1e3	59.32	59.94	30.36	30.52

B.3 Implementation Details

In the final step of Algorithm 1, we determine the hyperparameters for MDAA. The expansion layer dimension, denoted as φ , theoretically benefits from larger values. However, an excessively large dimension may introduce a significant number of parameters, occupying considerable computational resources. Given the constraints of our available GPU resources, we set the dimension of φ to 8000. The necessity of the parameter γ in Eq. 3 has been established in [35]. The model demonstrates stable performance over a wide range of γ values, indicating that as long as γ is within a reasonable range, its impact on the model's performance remains minimal. Table 8 shows the results under a sweep over six orders of magnitude (*i.e.*, $10^{-3}, 10^{-2}, \dots, 10^3$) using the same setting in the ablation study. The model performs robustly with a sufficient regularization, while collapses when the value of γ turns to be too extreme (larger than 10^3 and smaller than 10^{-2}). In this paper, we

Table 9: Comparison with SOTA methods on audio single-modality continual corruption task in terms of classification Top-1 accuracy (%), using dataset Kinetics50-C and VGGSound-C in severity level 5. The best results for each domain are highlighted in bold. * means we revise the method from BN to LN for fair comparison.

Method	Type	Kinetics50-C							VGGSound-C						
		Gauss.	Traff.	Crowd	Rain	Thund.	Wind	Avg.	Gauss.	Traff.	Crowd	Rain	Thund.	Wind	Avg.
		$t \rightarrow$							$t \rightarrow$						
Source	-	73.97	65.21	67.79	70.27	67.98	70.45	69.28	37.32	21.24	16.89	21.82	27.37	25.66	25.05
TENT*	TTA	74.44	68.04	71.30	70.25	72.53	70.35	71.15	10.76	1.15	0.40	0.32	0.51	0.31	2.24
SAR	TTA	73.88	65.68	68.00	70.91	69.07	70.45	69.66	37.39	8.57	7.03	12.58	10.77	13.71	15.01
EATA	CTTA	73.95	65.26	68.03	70.45	68.17	70.48	69.39	40.49	31.07	31.98	31.40	38.26	33.84	34.51
MMTTA*	MM-TTA	69.32	69.01	69.00	69.07	68.96	68.95	69.05	14.40	1.92	0.84	0.36	0.47	0.31	3.05
READ	MM-TTA	74.74	68.88	70.43	70.69	72.31	69.73	71.13	40.51	25.39	20.38	20.06	21.14	16.07	23.93
MDAA	MM-CTTA	73.33	71.99	73.36	73.26	74.24	73.76	73.32	38.57	34.57	34.37	34.30	37.40	35.70	35.82
		$t \leftarrow$							$t \leftarrow$						
Source	-	74.00	65.20	67.92	70.24	68.01	70.43	69.30	37.31	21.25	16.89	21.81	27.37	25.66	25.05
TENT*	TTA	73.31	70.00	71.57	70.30	68.87	71.09	70.86	0.37	0.30	0.30	0.31	0.97	3.73	1.00
SAR	TTA	73.29	66.79	68.14	70.71	67.97	70.36	69.55	32.02	9.92	7.04	9.49	11.41	16.03	14.32
EATA	CTTA	73.96	65.30	68.15	70.36	68.18	70.40	69.39	40.65	32.32	30.65	32.23	38.16	32.39	34.40
MMTTA*	MM-TTA	68.92	69.47	70.50	69.59	69.62	69.63	69.62	0.35	0.32	0.30	0.23	0.67	3.25	0.85
READ	MM-TTA	73.11	70.16	69.68	70.90	72.07	70.73	71.11	24.23	16.23	16.84	17.65	29.12	30.30	22.39
MDAA	MM-CTTA	72.55	73.67	72.98	73.04	73.18	71.55	72.83	38.59	35.35	34.50	34.31	36.94	34.91	35.77

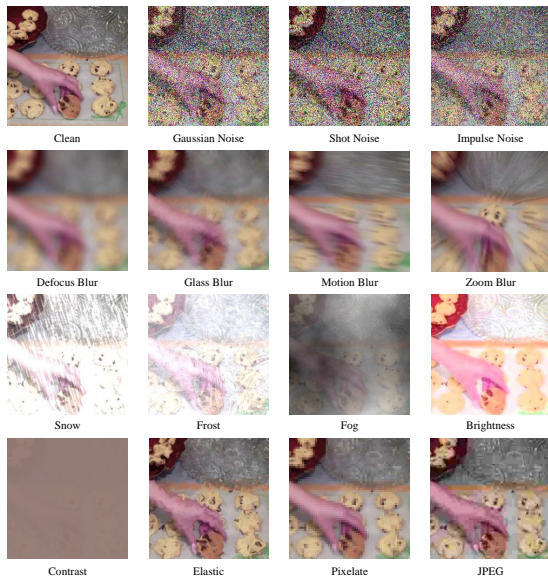


Figure 5: Visualization of 15 corruption types on the sampled video in Kinetics50-C benchmark.

set γ to 1 for Kinetics-50 and 10 for VGGSound. As discussed in Sections 4.2 and 4.3, the threshold θ in DLFM is fixed at 0.001 for both datasets, while the parameter n for reconstructing soft labels is set to 2 for Kinetics-50 and 7 for VGGSound. All experiments were conducted on an RTX3090 GPU, with results averaged over three runs.

C MORE EXPERIMENT RESULTS

In this appendix, we provide four more experiments for reference where Appendix C.1 and C.2 are the supplementary comparative

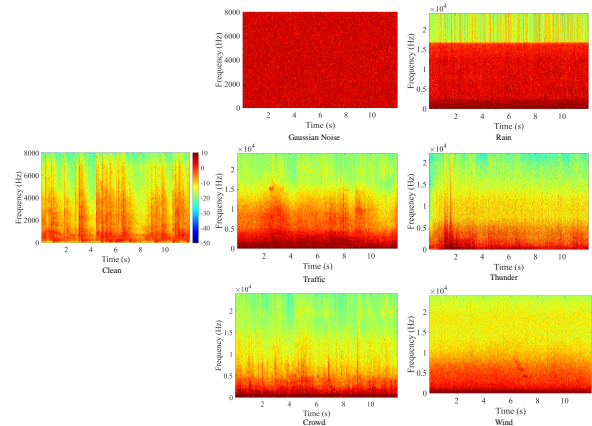


Figure 6: Spectrogram visualization of the clean audio and the corresponding 6 corruption types on the constructed Kinetics50-C benchmark. All Spectrogram use the same range of colorbar.

studies while Appendix C.3 is the further discussion on hyperparameters applied in MDAA.

C.1 Performance Comparison on Multi-modal Corruption

We follow the experimental setup in [27] to examine whether our model remains superior to others when the adaptation task is not continuous. In this section, the corrupted target domains are independent, and the results for corrupted audio and video modalities are presented in Tables 9, 10 and 11. The results show that the SOTA performance of MDAA is due not only to its ability to combat catastrophic forgetting, but also to its strong capacity to handle MM-TTA tasks effectively.

Table 10: Comparison with SOTA methods on video single-modality continual corruption task in terms of classification Top-1 accuracy (%), with dataset Kinetics50-C in severity level 5.

Method	Type	Gauss.	Shot.	Impul.	Defoc.	Glass.	Motion.	Zoom.	Snow	Frost	Fog	Bright.	Cont.	Elastic.	Pixel.	Jpeg	Avg.
$t \rightarrow$																	
Source	-	48.67	49.81	49.01	67.77	61.88	70.95	66.19	61.39	61.42	45.35	75.94	51.86	65.81	68.77	66.10	60.73
TENT*	TTA	48.53	48.65	46.06	62.91	62.15	65.77	63.83	54.78	54.64	33.79	36.79	19.86	11.75	3.82	3.38	41.11
SAR	TTA	48.48	49.87	48.71	66.92	62.56	70.58	66.77	59.25	60.50	47.19	75.34	50.77	65.23	66.91	64.01	60.21
EATA	CTTA	48.76	49.84	49.03	67.78	62.02	70.92	66.20	61.55	61.53	45.38	75.97	51.90	65.91	68.74	66.09	60.77
MMTTA*	MM-TTA	48.74	49.05	48.88	49.12	48.94	48.88	48.86	48.92	48.92	48.86	49.03	48.79	48.88	48.80	48.92	48.91
READ	MM-TTA	51.02	53.54	54.24	68.16	66.36	68.95	67.76	62.85	64.72	59.62	70.99	53.02	67.03	63.71	62.78	62.32
MDAA	MM-CTTA	55.84	55.79	55.50	64.29	63.71	68.04	68.10	66.06	68.01	65.71	72.97	66.36	70.04	70.51	70.53	65.43
$t \leftarrow$																	
Source	-	48.68	49.79	48.97	67.69	61.82	70.93	66.18	61.39	61.37	45.29	75.99	51.89	65.78	68.71	66.14	60.71
TENT*	TTA	41.93	47.19	49.22	64.80	64.33	68.05	63.86	61.42	62.12	51.65	73.92	50.80	67.47	69.03	66.80	60.17
SAR	TTA	48.08	49.07	48.83	66.25	63.02	70.39	66.27	59.53	60.31	46.28	75.62	51.23	65.47	68.47	66.14	60.33
EATA	CTTA	48.67	49.80	49.16	67.68	62.02	70.92	66.13	61.57	61.46	45.17	76.02	51.95	65.90	68.71	66.22	60.76
MMTTA*	MM-TTA	49.82	49.90	49.85	49.94	49.86	49.92	49.89	49.97	49.94	49.79	50.54	50.01	54.33	56.20	59.99	51.33
READ	MM-TTA	52.00	52.28	51.02	62.43	64.47	66.04	65.38	61.39	65.10	62.96	75.14	53.59	68.89	69.95	68.20	62.59
MDAA	MM-CTTA	70.55	70.43	70.08	71.81	70.30	72.19	70.88	69.38	69.35	67.48	73.16	62.07	68.63	67.98	65.21	69.30

Table 11: Comparison with SOTA methods on video single-modality continual corruption task in terms of classification Top-1 accuracy (%), with dataset VGGSound-C in severity level 5.

Method	Type	Gauss.	Shot.	Impul.	Defoc.	Glass.	Motion.	Zoom.	Snow	Frost	Fog	Bright.	Cont.	Elastic.	Pixel.	Jpeg	Avg.
$t \rightarrow$																	
Source	-	53.05	52.91	52.98	57.19	57.37	58.37	57.45	56.37	56.47	55.41	59.19	53.75	57.19	56.44	57.33	56.10
TENT*	TTA	53.27	52.76	52.00	54.58	54.35	55.04	54.86	52.59	52.81	53.11	53.50	50.80	53.03	52.31	52.14	53.14
SAR	TTA	53.14	53.29	53.21	56.95	56.91	58.41	57.47	56.10	56.78	56.34	58.35	53.98	57.27	55.93	56.48	56.04
EATA	CTTA	53.74	53.67	53.68	57.20	57.26	58.53	57.93	56.38	56.67	56.23	59.04	53.63	58.19	57.36	57.48	56.47
READ	MM-TTA	53.77	54.26	54.28	58.04	58.00	59.09	58.84	57.43	58.18	58.12	59.38	55.99	58.30	57.51	57.91	57.27
MDAA	MM-CTTA	55.63	55.91	55.88	57.50	57.77	58.27	57.84	57.05	56.72	56.77	58.67	55.78	57.55	56.87	57.84	57.07
$t \leftarrow$																	
Source	-	53.01	52.88	52.97	57.20	57.42	58.41	57.49	56.37	56.49	55.43	59.16	53.74	57.19	56.42	57.29	56.10
TENT*	TTA	50.48	50.50	50.50	53.09	53.19	53.70	53.18	52.31	53.47	53.57	55.40	52.22	56.23	56.74	56.99	53.44
SAR	TTA	53.02	52.95	52.71	56.78	56.63	58.18	57.38	55.97	56.69	56.45	58.46	54.03	57.41	56.53	57.16	56.02
EATA	CTTA	53.69	53.66	53.61	57.26	57.34	58.46	57.84	56.35	56.82	56.72	59.21	54.10	58.28	57.39	57.54	56.55
READ	MM-TTA	55.33	55.34	54.93	58.16	57.88	58.82	58.50	57.24	57.94	57.86	59.65	55.67	58.79	57.87	58.10	57.47
MDAA	MM-CTTA	55.85	55.87	55.94	57.40	57.85	58.25	57.95	57.02	56.89	56.68	58.66	55.84	57.58	56.92	58.00	57.11

C.2 Performance Comparison on Single-modality Continual Corruption

In this section, we compare the performance of each method under single-modality corruption. This task is similar to the **progressive single-modality corruption** task described in the main text, but here we use a batch size of 64.

C.3 Dynamic threshold update

The threshold θ we used in DLFM is a fixed number. In this section we attempt to update θ in a dynamic way during the adaptation. We define the threshold θ_t^i for classifier i in time t as

$$\theta_t^i = \begin{cases} \theta_{t-1}^i + \lambda (d_t^i - d_{t-1}^i) & , \text{if } t > 1 \\ \theta_{ini} & , \text{if } t = 1 \end{cases}, i = \{a, v, m\} \quad (11)$$

$$d_t^i = \frac{\sum_{k=1}^{N_k} (\max(p_k^{leader}) - \max(p_k^i))}{N_k}, i = \{a, v, m\}, \quad (12)$$

Table 15: Ablation studies on parameter λ .

λ	KS-video		VGG-audio	
	\rightarrow	\leftarrow	\rightarrow	\leftarrow
0	63.55	69.54	34.37	34.35
0.01	63.49	69.31	34.35	34.30
0.05	63.36	69.43	34.38	34.31
0.1	63.18	69.42	34.40	34.29
0.2	62.93	69.33	34.41	34.31

where λ is the learning rate, θ_{ini} is the initial threshold and N_k is the batch size. d_t^i is calculated to reflect the gap between *Leader* and *follower* i . The original intention is to adjust the threshold size according to d_t changes to eliminate statistical bias across domains. However, as shown in Table 15, this approach achieves lower performance while requiring more variables to be memorized. Therefore, only the fixed threshold is used in the formal method.

D PROOFS OF THEOREMS

Proof of Theorem 1. known the optimal problem in Eqn.6 can be further written as:

$$\begin{aligned} & \underset{\mathbf{W}_{Tg,t}}{\operatorname{argmin}} \sum_{k=1}^{N_{Sr}} \omega_k (\mathbf{y}_{Sr,k} - \mathbf{x}_{\text{exf},k} \mathbf{W}_{Tg,t})^\top (\mathbf{y}_{Sr,k} - \mathbf{x}_{\text{exf},k} \mathbf{W}_{Tg,t}) + \left(\tilde{\mathbf{Y}}_{Tg,1:t} - \mathbf{X}_{\text{exf},1:t} \mathbf{W}_{Tg,t} \right)^\top \left(\tilde{\mathbf{Y}}_{Tg,1:t} - \mathbf{X}_{\text{exf},1:t} \mathbf{W}_{Tg,t} \right) + \gamma \mathbf{W}_{Tg,t}^\top \mathbf{W}_{Tg,t} \\ & = \underset{\mathbf{W}_{Tg,t}}{\operatorname{argmin}} \sum_{k=1}^{N_{Sr}} \omega_k (\mathbf{W}_{Tg,t}^\top \mathbf{x}_{\text{exf},k}^\top \mathbf{x}_{\text{exf},k} \mathbf{W}_{Tg,t} - \mathbf{y}_{Sr,k}^\top \mathbf{x}_{\text{exf},k} \mathbf{W}_{Tg,t} - \mathbf{W}_{Tg,t}^\top \mathbf{x}_{\text{exf},k}^\top \mathbf{y}_{Sr,k} + \mathbf{y}_{Sr,k}^\top \mathbf{y}_{Sr,k}) + \\ & \quad (\mathbf{W}_{Tg,t}^\top \mathbf{X}_{\text{exf},1:t}^\top \mathbf{X}_{\text{exf},1:t} \mathbf{W}_{Tg,t} - \tilde{\mathbf{Y}}_{Tg,1:t}^\top \mathbf{X}_{\text{exf},1:t} \mathbf{W}_{Tg,t} - \mathbf{W}_{Tg,t}^\top \mathbf{X}_{\text{exf},1:t}^\top \tilde{\mathbf{Y}}_{Tg,1:t} + \tilde{\mathbf{Y}}_{Tg,1:t}^\top \tilde{\mathbf{Y}}_{Tg,1:t}) + \gamma \mathbf{W}_{Tg,t}^\top \mathbf{W}_{Tg,t}. \end{aligned}$$

Note above equation as L_1 , derive L_1 for $\mathbf{W}_{Tg,1:t}$ as

$$\begin{aligned} \frac{\partial L_1}{\partial \mathbf{W}_{Tg,t}} &= 2 \sum_{k=1}^{N_{Sr}} \omega_k (\mathbf{x}_{\text{exf},k}^\top \mathbf{x}_{\text{exf},k} \mathbf{W}_{Tg,t} - \mathbf{x}_{\text{exf},k}^\top \mathbf{y}_{Sr,k}) + (\mathbf{X}_{\text{exf},1:t}^\top \mathbf{X}_{\text{exf},1:t} \mathbf{W}_{Tg,t} - \mathbf{X}_{\text{exf},1:t}^\top \tilde{\mathbf{Y}}_{Tg,1:t}) + 2\gamma \mathbf{W}_{Tg,t} \\ &= 2 \sum_{k=1}^{N_{Sr}} (\tilde{\mathbf{x}}_{\text{exf},k}^\top \tilde{\mathbf{x}}_{\text{exf},k} \mathbf{W}_{Tg,t} - \tilde{\mathbf{x}}_{\text{exf},k}^\top \tilde{\mathbf{y}}_{Sr,k}) + (\mathbf{X}_{\text{exf},1:t}^\top \mathbf{X}_{\text{exf},1:t} \mathbf{W}_{Tg,t} - \mathbf{X}_{\text{exf},1:t}^\top \tilde{\mathbf{Y}}_{Tg,1:t}) + 2\gamma \mathbf{W}_{Tg,t} \\ &= 2(\tilde{\mathbf{X}}_{\text{exf},k}^\top \tilde{\mathbf{X}}_{\text{exf},k} \mathbf{W}_{Tg,t} + \mathbf{X}_{\text{exf},1:t}^\top \mathbf{X}_{\text{exf},1:t} \mathbf{W}_{Tg,t} - \tilde{\mathbf{X}}_{\text{exf},k}^\top \tilde{\mathbf{Y}}_{Sr,k} - \mathbf{X}_{\text{exf},1:t}^\top \tilde{\mathbf{Y}}_{Tg,1:t}) + 2\gamma \mathbf{W}_{Tg,t} \\ &= 0. \end{aligned}$$

Therefore

$$\begin{aligned} \hat{\mathbf{W}}_{Tg,t} &= (\tilde{\mathbf{X}}_{\text{exf},Sr}^\top \tilde{\mathbf{X}}_{\text{exf},Sr} + \mathbf{X}_{\text{exf},1:t}^\top \mathbf{X}_{\text{exf},1:t} + \gamma \mathbf{I})^{-1} (\tilde{\mathbf{X}}_{\text{exf},Sr}^\top \tilde{\mathbf{Y}}_{Sr} + \mathbf{X}_{\text{exf},1:t}^\top \tilde{\mathbf{Y}}_{Tg,1:t}) = \mathbf{P}_{Tg,t}^{-1} \mathbf{Q}_{Tg,t}, \\ \mathbf{P}_{Tg,t} &= \mathbf{P}_{Sr} + \mathbf{X}_{\text{exf},1:t}^\top \mathbf{X}_{\text{exf},1:t} = \mathbf{P}_{Tg,1} + \mathbf{X}_{\text{exf},2:t}^\top \mathbf{X}_{\text{exf},2:t} = \cdots = \mathbf{P}_{Tg,t-1} + \mathbf{X}_{\text{exf},t}^\top \mathbf{X}_{\text{exf},t}, \\ \mathbf{Q}_{Tg,t} &= \mathbf{Q}_{Sr} + \mathbf{X}_{\text{exf},1:t}^\top \tilde{\mathbf{Y}}_{Tg,1:t} = \mathbf{Q}_{Tg,1} + \mathbf{X}_{\text{exf},2:t}^\top \tilde{\mathbf{Y}}_{Tg,2:t} = \cdots = \mathbf{Q}_{Tg,t-1} + \mathbf{X}_{\text{exf},t}^\top \tilde{\mathbf{Y}}_{Tg,t}. \end{aligned}$$

Received 9 April 2025; revised 12 Jun 2025; accepted 6 July 2025